

# **CO<sub>2</sub> CAPTURE USING 3D PRINTED PIM-1 INCORPORATING SOLID ADSORBENTS**

A Thesis  
Presented to  
The Academic Faculty

by

Nathan Sidhu

In Partial Fulfillment  
of the Requirements for the Degree  
Bachelor of Science in the  
School of Chemical and Biomolecular Engineering

Georgia Institute of Technology  
May 2018

# **CO<sub>2</sub> CAPTURE USING 3D PRINTED PIM-1 INCORPORATING SOLID ADSORBENTS**

Approved by:

Dr. Ryan Lively, Advisor  
School of Chemical and Biomolecular Engineering  
*Georgia Institute of Technology*

Dr. Victor Breedveld  
School of Chemical and Biomolecular Engineering  
*Georgia Institute of Technology*

Dr. Carson Meredith  
School of Chemical and Biomolecular Engineering  
*Georgia Institute of Technology*

Date Approved: April 24<sup>th</sup>, 2018



## **ACKNOWLEDGEMENTS**

I wish to thank Dr. Ryan Lively, for his invaluable guidance throughout my undergraduate research career. I also wish to thank Fengyi Zhang for his mentorship during this project. Lastly, I would like to thank my mother and father, without whose support and encouragement I would not be here.

## TABLE OF CONTENTS

	Page
ACKNOWLEDGEMENTS	iii
LIST OF FIGURES	v
ABSTRACT	1
INTRODUCTION	2
METHODS AND MATERIALS	6
RESULTS AND DISCUSSION	11
CONCLUSIONS AND FUTURE WORK	15
REFERENCES	17

## LIST OF FIGURES

	Page
Figure 1: CO <sub>2</sub> adsorption by 3D-printed adsorbent	4
Figure 2: 3D printing set up	5
Figure 3: Solid adsorbent framework structures	6
Figure 4: Schematic overview of 3D-printing device	9
Figure 5: SEM scan of synthesized Mg-MOF-74	11
Figure 6: Adsorption isotherm of synthesized Mg-MOF-74	12
Figure 7: Pure PIM-1 3D print	13
Figure 8: Cellulose acetate / 13X storage and loss moduli	13

## ABSTRACT

Rising atmospheric CO<sub>2</sub> concentration has exceeded nature's carbon recycling capacity and caused severe environmental hazards. To capture CO<sub>2</sub> from point sources and from atmospheric air, various solid CO<sub>2</sub> adsorbents, including zeolites, metal organic frameworks (MOFs) and immobilized amines, have been developed. While this has been a promising development, the discrete nature of the solid adsorbents limits their applications without the use of a substrate. To reduce energy cost of direct air capture, it is important to develop a structured adsorbent with both high adsorbent efficiency and low gas pressure drop. In this work, we proposed a 3D-printing technique to manufacture a structured CO<sub>2</sub> adsorbent, in which a solid adsorbent is supported by a highly permeable polymer with intrinsic microporosity (PIM-1). This method of adsorbent development allows for customizable substrate patterning and sizing, thereby allowing for the transport properties through the adsorbent to be tuned. Compared with existing 3D-printing techniques for structured adsorbent manufacture, our technique features mild activation conditions and low internal mass transfer resistance. The solid adsorbents selected for the study include Mg-MOF-74, HKUST-1, and Zeolite 13X. Rheological studies were performed to determine the optimal loading compositions for the polymer-adsorbent inks and these inks were successfully printed.

## INTRODUCTION

Industrialization has transformed the way in which society operates, bringing about new levels of efficiency production methods and improving standards of living; however, the associated release of greenhouse gases to the atmosphere have brought about detrimental environmental changes. If unchecked, greenhouse gas emissions, particularly of CO<sub>2</sub>, are predicted to bring about a global surface temperature rise between 3.7 °C and 4.8 °C by 2100.<sup>1</sup> The present levels of climate change have already had far reaching impacts. Water resources have been altered due to persistent changes in precipitation and melting snow or ice. Land and water based species have seen changes to their geographic range and migration patterns among others. Humans systems are also heavily impacted, with increases in global temperature extremes and the number of heavy participation events being linked to global warming.<sup>1</sup> These are only a small sample of the consequences of climate change and despite these evident changes on a global scale, emissions have not decreased. Between 2010 and 2014, global carbon emissions due to fossil fuel rose from 9,137 million tons to an estimated 9,853 million tons, equivalent to 33,478 to 36,100 million tons of CO<sub>2</sub>.<sup>2</sup> This level of carbon release simply cannot be handled by nature and has caused a climb in atmospheric CO<sub>2</sub> levels. For the 10,000 years prior to the mid-18th century, CO<sub>2</sub> levels were constant at approximately 280 ppm.<sup>3</sup> As of August 2017, atmospheric CO<sub>2</sub> levels have risen to levels over 400 ppm.<sup>4</sup> With 65% of global emissions coming from fossil fuels and industrial processes,<sup>5</sup> a heavy focus is being placed on eliminating carbon release from these sources.



While green energy sources are being developed and will eventually replace fossil fuels, this transition will be slow and the reliance on fossil fuels will not change for the foreseeable future. As such, there is a focus on developing low-energy separation methods that are efficient and scalable, with technologies such as selective adsorbents being of great interest. Currently developed methods for capturing carbon from fossil fuels are already in use, but they suffer from high costs, low efficiency, or other technological limitations. Prior to combustion, a fossil fuel may be reacted with oxygen, air, and/or steam to generate syngas, a gaseous mixture of carbon monoxide and hydrogen. The syngas is then used in a water gas-shift reactor to generate CO<sub>2</sub> and hydrogen. The CO<sub>2</sub> generated in this process is readily separated due to its high concentration, leaving a purified H<sub>2</sub> fuel for further use.<sup>6</sup> During combustion, a method known as oxy-fuel combustion may be used. Here, fossil fuel combustion occurs with pure or nearly pure oxygen. CO<sub>2</sub> and H<sub>2</sub>O are the majority components of the flue gas from oxy-fuel combustion and separation of CO<sub>2</sub> is fairly easy. This is relatively expensive process, however, as pure oxygen generation relies on cryogenic air separation.<sup>6</sup> Additionally, post-combustion separation can be used to separate CO<sub>2</sub>. Fossil fuels are combusted with air, and the generated flue gas is processed to capture and store CO<sub>2</sub>, using chemical sorbents.<sup>6</sup> Post-combustion separations are of particular interest as they may be integrated into existing systems, without the requirement of significant redesign; however, current processes leave much to be desired due to cost, chemical sensitivity, and overall performance limitations.

Intrinsically low-energy separation processes for carbon capture are preferred. Any process requiring significant energy input will work directly against the aim of

reducing carbon emissions. Two commonly used methods for CO<sub>2</sub> are liquid amine absorption and carbonation-calcination. Various aqueous solutions of amines, such as monoethanolamine, are used in liquid amine absorption to capture CO<sub>2</sub>. While this process is efficient for CO<sub>2</sub> capture, it is highly sensitive to common impurities such as SO<sub>2</sub> and NO<sub>x</sub>, liquid amines are highly corrosive, and significant energy input is required during regeneration.<sup>7</sup> In carbonation-calcination, CO<sub>2</sub> and CaO are reacted to form CaCO<sub>3</sub> and the opposite reaction is then performed. This process is not sensitive to SO<sub>2</sub>, however, both reactions require high energy input due to the high reaction temperature.<sup>7</sup>

In an effort to reduce these energy costs and develop a more robust process, it is proposed to instead use a solid adsorbent to capture CO<sub>2</sub> requiring only minimal energy costs. A basic overview of this process is detailed in Figure 1.

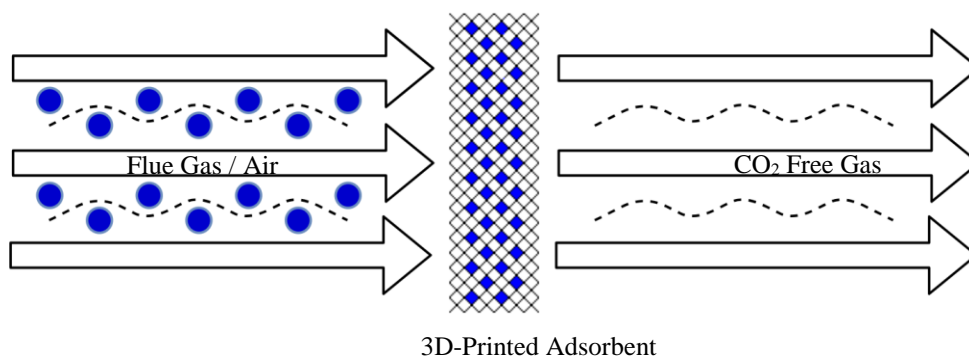


**Figure 1.** CO<sub>2</sub> (blue) adsorption by a 3D-printed adsorbent

Specifically, this work used a combined material consisting of a microporous substrate (PIM-1) with an integrated solid CO<sub>2</sub> adsorbent, such as Zeolite 13X, HKUST-1, or Mg-MOF-74, in a 3D-printed configuration. In this project, the chosen carbon capture materials were combined with a PIM-1 at varying composition levels and implemented using a 3D-printing technique. Our method of 3D printing features a mild activation

condition to develop a unique structure which has been shown to prevent structural deformation. An overview of the 3D-printing device may be seen in Figure 2.

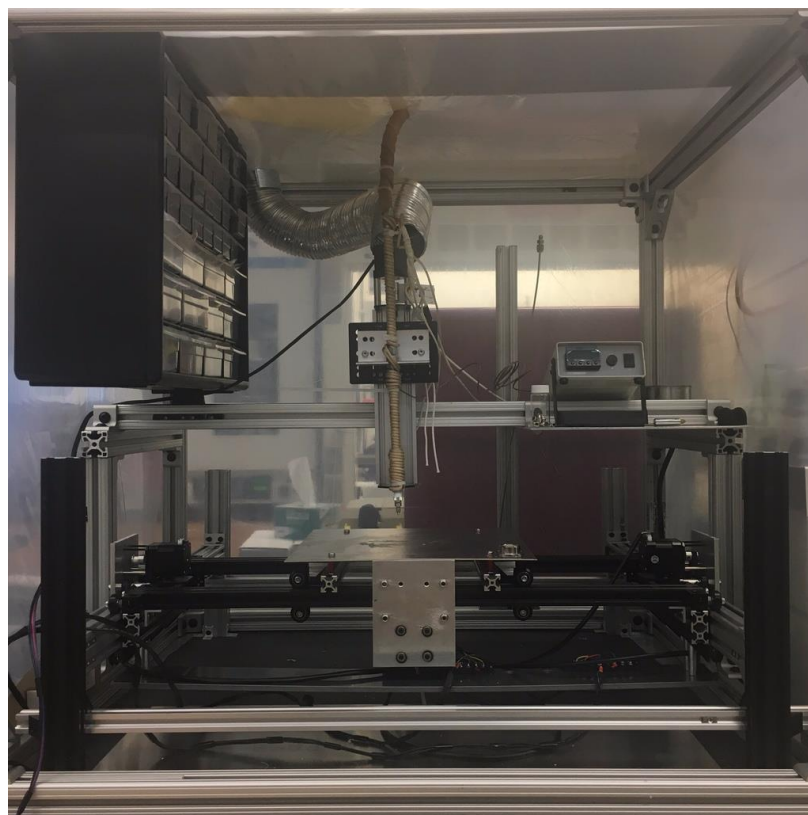


**Figure 2.** 3D printing set up

Size control of MOFs was the first focus of the study. To provide uniform inks, crystals on the order of 1 micron were developed and implemented into the substrate. The complex modulus and viscosity of the printed adsorbents were studied to fully evaluate the structural properties of the polymer-adsorbent inks to determine optimal loading compositions.

## METHODS AND MATERIALS

Three CO<sub>2</sub> adsorbents have been selected for use in this study: Zeolite 13X, HKUST-1, and Mg-MOF-74 (Figure 3). These materials were selected for their demonstrated ability to adsorb CO<sub>2</sub> and due to their relative ease of synthesis,<sup>8-9</sup> with Zeolite 13X being a commercially available adsorbent and implemented as the baseline material for much of this work. Careful synthesis procedures were followed in order to carefully control the size of the crystalline adsorbents.

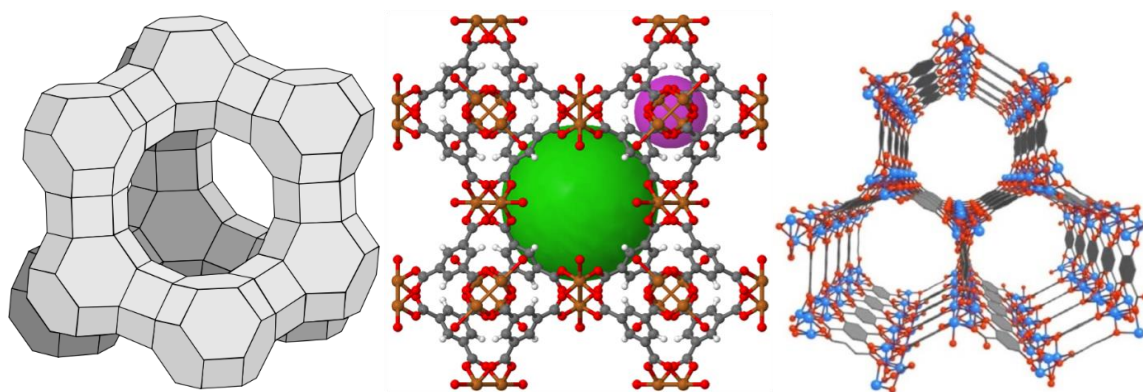


**Figure 3.** Framework structures of (left to right) Zeolite 13X, HKUST-1, and Mg-MOF-74.<sup>10-12</sup>

### *Mg-MOF-74*

For the synthesis of Mg-MOF-74, the method proposed by Glover et al.<sup>9</sup> was used as a basis. With stirring, 0.100 g of dihydroxyterephthalic acid (DHTA) and 0.512 g of Mg(NO<sub>3</sub>)<sub>2</sub> 6H<sub>2</sub>O were combined in 45 mL of N,N dimethylformamide (DMF), 3 mL of H<sub>2</sub>O, and 3 mL of ethanol. The solution was stirred for approximately 10 minutes at 300 RPM before being transferred in equal parts to two 45 mL Teflon lined autoclaves and cooked at 125 °C for 21 hours with rotation. The autoclaves were quenched in a water bath and the resultant crystals were recovered via scraping and washing with methanol.

The crystals were repeatedly soaked in methanol and recovered via centrifugation over a period of three days, followed by activation at 180 °C for 12 hours.

#### *HKUST-1*

For the synthesis of HKUST-1, the method proposed by Petit et al.<sup>13</sup> was used as a basis. With stirring, 5 g of copper nitrate hemipentahydrate and 2.5 g of 1,3,5 benzenetricarboxylic acid were combined in 42.5 mL of DMF for approximately 5 min, followed by the addition of 42.5 mL ethanol and continued stirring for 5 min. Then, 42.5 mL of H<sub>2</sub>O was added and the solution was stirred for 30 min until all crystals were dissolved. Half of the mother solution was then transferred in equal parts to Teflon lined autoclaves and cooked at 85 °C for 24 hours with rotation. The autoclaves were quenched in a water bath and the resultant crystals were recovered via vacuum filtration. The remaining half of the solution was decanted into a round-bottom flask and cooked at 60 °C for 24 hours with stirring. The resultant crystals were recovered via centrifugation. All crystals were then soaked in dichloromethane (DCM) with stirring, refreshing the DCM every 24 hours, for three days followed by activation at 180 °C for 12 hours. The HKUST-1 crystals produced were stored in a desiccator.

#### *PIM-1 Polymer Solutions*

The method describe by Jue et al.<sup>14</sup> was followed to synthesize PIM-1. The synthesized PIM-1 was then sequentially washed in dimethylformamide (DMF) and methanol. The PIM-1 powder was activated at 80 °C in a vacuum oven for 12 hours prior to preparation of polymer solutions. Due to the water sensitivity of PIM-1, exposure to water was eliminated by preparing the polymer solutions, consisting of solvent, nonsolvent and polymer, inside a sealed stainless-steel cartridge made of Swagelok tube

fittings. The cartridges were heated at 50 °C for 12 hours with rotation, ensuring the preparation of a homogenous solution and full dissolution of PIM-1. These cartridges were loaded onto the custom 3D printer (Figure 2).

### *Rheology Characterization*

Rheological characterization of the 3D-printing inks were performed on an Anton Paar MCR 302 Rheometer (Anton Paar GmbH, Austria-Europe) with couette geometry. The measuring bob diameter is 16.66 mm and the measuring cup diameter is 18.07 mm. To prevent the sample from evaporating, a cap with the appropriate coquette is installed and loaded with tetrahydrofuran (THF), refreshing the THF periodically. The 3D inks are prepared for measurement by heating to 50 °C, followed by cooling to room temperature, to ensure they are homogenous. For viscometry measurements, a range of shear rates from 0.01 s<sup>-1</sup> to 100 s<sup>-1</sup> was used. Oscillatory measurements are carried out at frequency sweep mode (strain amplitude fixed at 0.1 while angular frequency ranging from 0.01 rad/s to 628 rad/s) and amplitude sweep mode (angular frequency fixed at 1 rad/s while strain amplitude ranging from 0.01 to 10).

### *Solution-based 3D Printing*

All printed PIM-1 adsorption devices are produced using a custom-built Cartesian 3D printer (Openbuilds) that processes the optimized inks (Figure 4). Appropriate G-code commands were written to control movement of 3D printer. The ink is extruded through a stainless-steel needle 410 µm inner diameter nozzle (G24, inner diameter is 311µm) by applying the appropriate pressure, which is controlled by a regulator.



**Figure 4.** Schematic diagram of 3D-printing device: (1) Printing surface, (2) controlled atmosphere chamber, (3) printing nozzle, and (4) printing ink.

#### *Adsorption Performance Test*

Kinetic adsorption experiments were conducted to investigate the mass transfer resistance within adsorbent/PIM-1 composites of different geometry and microstructure. Samples of interest were placed in the chamber of Dynamic Vapor Sorption System (Surface Measurement Systems) where  $\text{CO}_2$  with specific pressure was generated. Mass change of sample during exposure to  $\text{CO}_2$  was monitored.

$\text{CO}_2$  isotherms of pristine solid adsorbent and adsorbent/PIM-1 composite were also measured utilizing Dynamic Vapor Sorption System. Sample being tested was exposed to a series of  $\text{CO}_2$  pressure.

To reveal the significance of 3D-printed sorbent for industrial application. PIM-1 adsorption module was assembled by fixing a 3D-printed PIM-1 monolith into a customized stainless steel enclosure.  $\text{CO}_2/\text{N}_2$  mixture flows through the adsorption column. Outlet gas is analyzed online by a quadrupole mass spectrometer, Omnistar GSD

301 C (Pfeiffer Vacuum). Before each run, the PIM-1 adsorption column was heated to 100°C under vacuum for 12 hours to get rid of residual gases.

#### *Nitrogen Physisorption*

BET surface areas of PIM-1 and synthesized adsorbent samples were obtained from nitrogen physisorption experiments at 77 K using a BELSORP-max (MicrotracBEL). Before measurement, PIM-1 samples were refreshed by methanol to eliminate aging effects.

#### *Mercury Porosimetry*

Mercury porosimetry were used to reveal the hierarchical pore structure of 3D-printed PIM-1 scaffold. The scaffold were refreshed with methanol and then measured by AutoPore IV (Micromeritics).



## RESULTS AND DISCUSSION

### *Crystal Synthesis and Characterization*

A primary objective of this work was to develop size controlled crystals of the proposed adsorbents, particularly Mg-MOF-74. In the size control experiments of the crystals, the target 1 – 2  $\mu\text{m}$  scale was achieved for Mg-MOF-74 (Figure 5). Having achieved crystals within our target size range, to provide polymer inks of uniform concentration, the Mg-MOF-74 samples were then characterized for surface area and adsorption capacity.

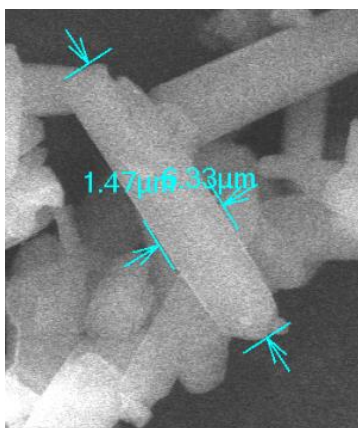


**Figure 5.** SEM scan of synthesized Mg-MOF-74

Initial characterization results revealed that Mg-MOF-74 did not possess the adsorption properties expected. This shown by the reduced uptake of  $\text{CO}_2$  (Figure 6).

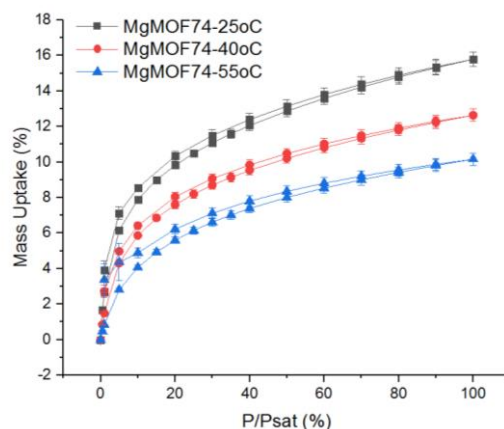


**Figure 6.** Adsorption isotherms of synthesized Mg-MOF-74.

At 25 °C, it was expected to have an uptake of approximately 27.5 wt.%,<sup>15</sup> but only 16 wt.% uptake was achieved. This is consistent with surface area analysis. It was hypothesized the reduced adsorption and surface area was due to trapped linkers in the structure, due to the sole use of MeOH to wash the synthesized Mg-MOF-74. This led to a change in the washing procedure, using anhydrous DMF, followed by anhydrous MeOH, in place of only MeOH. DMF was added to the washing procedure as it is an applicable solvent for all the starting materials. In addition, there was the potential for degradation of the Mg-MOF-74 structure due to the presence of water. While it is not expected that water sensitivity is a dominant feature of Mg-MOF-74, anhydrous solvents were used post-synthesis and samples were stored in a desiccator to minimize water exposure prior to characterization. As such, pristine Mg-MOF-74 samples could be characterized and accurately compared to literature.

### *3D Printing of Polymer-Adsorbent Inks*

PIM-1 was successfully printed using the custom built 3D-printing module. A preliminary structure is shown in Figure 7.

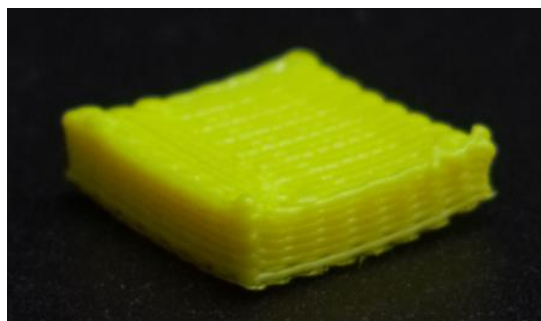


**Figure 7.** Pure PIM-1 3D print

Having developed a reliable printing method for the pure PIM-1, rheological studies were then performed to determine the effect of adsorbent packing on an ink. In these studies mixtures of cellulose acetate (CA), acetone, and Zeolite 13X were first used. CA performs similarly to PIM-1, but is significantly cheaper, and Zeolite 13X is the cheapest and most readily available of three adsorbents chosen. The weight ratio of 13X to CA was held constant at 10:1, while the weight ratio of acetone to CA was varied between 12:1 and 6:1. The properties of interest were the storage modulus ( $G'$ ) and the loss modulus ( $G''$ ), where a greater value of  $G'$  indicates a material with more solid characteristic and a greater value of  $G''$  indicates a material with more liquid characteristic. The results of the CA/Acetone/13X inks may be seen in Figure 8.

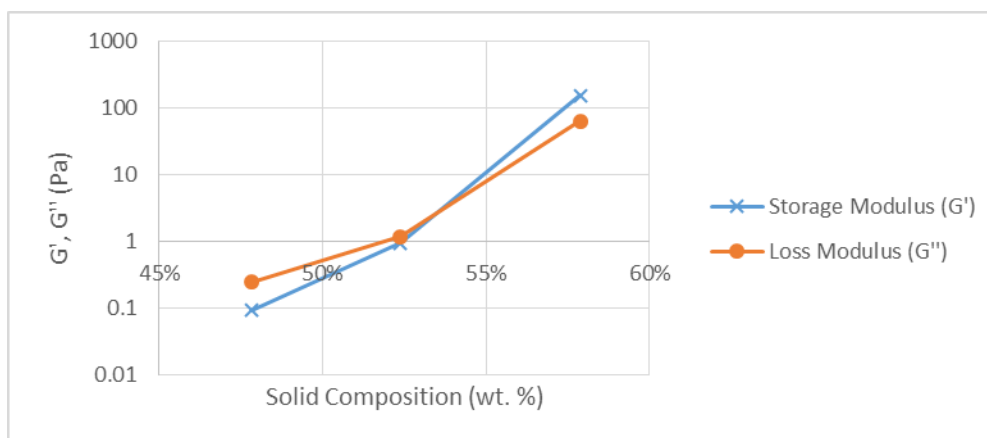


**Figure 8.** Comparison of storage and loss moduli at varying solid compositions.

A critical point is the cross over point between the storage and loss modulus as the solid composition increases, which occurred at approximate 52 wt. %. Based upon empirical evaluation of the operating range of pure PIM-1 inks, reducing the solids composition from the cross over point by ~5% gives a good initial starting composition to fine tune the inks. These compositions, ~5% below the cross over point were seen to be optimal as the inks possessed a low enough viscosity to flow easily enough to be printed (pressures less than ~2000 kPa), while not being too low so as to maintain its shape during printing and drying, giving the desired monolith geometry. CA/13X were successfully printed at compositions close to 47 wt. % solids, and this composition will be used as a starting point for PIM-1 / adsorbent inks.

## CONCLUSIONS AND FUTURE WORK

To create adsorbents with customizable structures for optimal flow configurations, a novel 3D-printing process was developed. Using a mild activation, to prevent structural deformation, this process was used to successfully print structures of neat PIM-1 in a desired monolithic structure. This work was then expanded to polymer/adsorbent inks, beginning with CA/13X. Rheological studies were undertaken to characterize the degree of solid-like and liquid-like properties, as described by the relative values of the storage modulus and loss modulus. It was found that at values below ~52 wt. % solids (polymer and adsorbent), the samples possessed more liquid-like properties. By reducing the solids concentration by ~5%, the concentration reduction found to be effective in the neat PIM-1 printing working, the CA/13X inks were successfully printed. This work has provided a composition target range for the PIM-1/adsorbent inks which are to be developed.

To perform the desired capture of CO<sub>2</sub> using a 3D-printed adsorbent, the adsorbents of interest, Mg-MOF-74 and HKUST-1, had to be fine-tuned. In particular, it is desired to have adsorbent crystals on the order of 1 – 2  $\mu\text{m}$ , to ensure uniform distribution within the polymer inks. This size range was successfully hit for Mg-MOF-74; however, the CO<sub>2</sub> uptake capability was severely dampened compared to reported values, being reduced from 27.5 wt. % to 16 wt. %. It was hypothesized that this was due to the presence of trapped linker ligands and, to a lesser degree, structural degradation due to water exposure. The washing procedure was modified to implement anhydrous DMF and anhydrous MeOH, to more readily removed trapped linker ligands and any

other synthesis components and minimize water exposure. The next steps of the work will be to re-characterize the newly synthesized Mg-MOF-74 samples and perform the same characterization work on the synthesized HKUST-1 samples. Once the uptake performance is verified, the adsorbents may then be implemented into the inks, to begin the fine tuning of the 3D-printing process and performance characterization of the printed adsorbents.

## REFERENCES

1. Pachauri, R. K.; Allen, M. R.; Barros, V. R.; Broome, J.; Cramer, W.; Christ, R.; Church, J. A.; Clarke, L.; Dahe, Q.; Dasgupta, P., *Climate change 2014: synthesis report. Contribution of Working Groups I, II and III to the fifth assessment report of the Intergovernmental Panel on Climate Change*. IPCC: 2014.
2. Boden, T.; Marland, G.; Andres, R., Global, Regional, and National Fossil-Fuel CO<sub>2</sub> Emissions (2010) Carbon Dioxide Information Analysis Center. *Oak Ridge National Laboratory, USA doi* **2016**, 10.
3. Eggleton, T., *A Short Introduction to Climate Change*. 1st ed.; Cambridge University Press: Cambridge, 2013.
4. Tans, P.; Keeling, R. Trends in Atmospheric Carbon Dioxide. <https://www.esrl.noaa.gov/gmd/ccgg/trends/> (accessed Nov 25).
5. EPA Greenhouse Gas Emissions. <https://www.epa.gov/ghgemissions/global-greenhouse-gas-emissions-data> (accessed November 20).
6. Sanz-Pérez, E. S.; Murdock, C. R.; Didas, S. A.; Jones, C. W., Direct Capture of CO<sub>2</sub> from Ambient Air. *Chemical Reviews* **2016**, 116 (19), 11840-11876.
7. Metz, B.; Davidson, O.; De Coninck, H.; Loos, M.; Meyer, L., IPCC, 2005: IPCC special report on carbon dioxide capture and storage. Prepared by Working Group III of the Intergovernmental Panel on Climate Change. *Cambridge, United Kingdom and New York, NY, USA* **2005**, 442.
8. Kumar, A.; Madden, D. G.; Lusi, M.; Chen, K. J.; Daniels, E. A.; Curtin, T.; Perry, J. J.; Zaworotko, M. J., Direct Air Capture of CO<sub>2</sub> by Physisorbent Materials. *Angewandte Chemie-International Edition* **2015**, 54 (48), 14372-14377.
9. Grant Glover, T.; Peterson, G. W.; Schindler, B. J.; Britt, D.; Yaghi, O., MOF-74 building unit has a direct impact on toxic gas adsorption. *Chemical Engineering Science* **2011**, 66 (2), 163-170.
10. Faujasite structure2. Wikipedia: 2011.
11. HKUST-1. University of Liverpool.
12. MgMOF74. Lawrence Berkeley National Laboratory: 2013.
13. Petit, C.; Burrell, J.; Bandoz, T. J., The synthesis and characterization of copper-based metal-organic framework/graphite oxide composites. *Carbon* **2011**, 49 (2), 563-572.
14. Jue, M. L.; McKay, C. S.; McCool, B. A.; Finn, M.; Lively, R. P., Effect of Nonsolvent Treatments on the Microstructure of PIM-1. *Macromolecules* **2015**, 48 (16), 5780-5790.
15. Trickett, C. A.; Helal, A.; Al-Maythalony, B. A.; Yamani, Z. H.; Cordova, K. E.; Yaghi, O. M., The chemistry of metal-organic frameworks for CO<sub>2</sub> capture, regeneration and conversion. *Nature Reviews Materials* **2017**, 2, 17045.